RSC Advances

Accepted Manuscript

This article can be cited before page numbers have been issued, to do this please use: M. Hasanzadeh, A. Bahrami, M. Alizadeh and N. Shadjou, *RSC Adv.*, 2013, DOI: 10.1039/C3RA42393J.

View Article Online
DOI: 10.1039/C3RA42393J

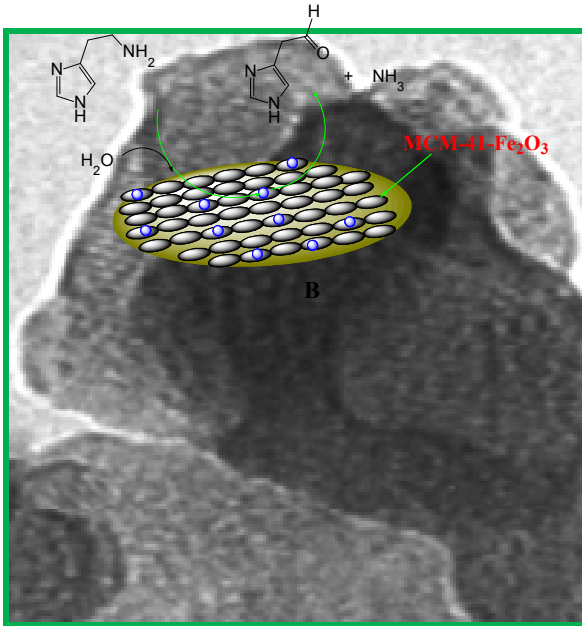

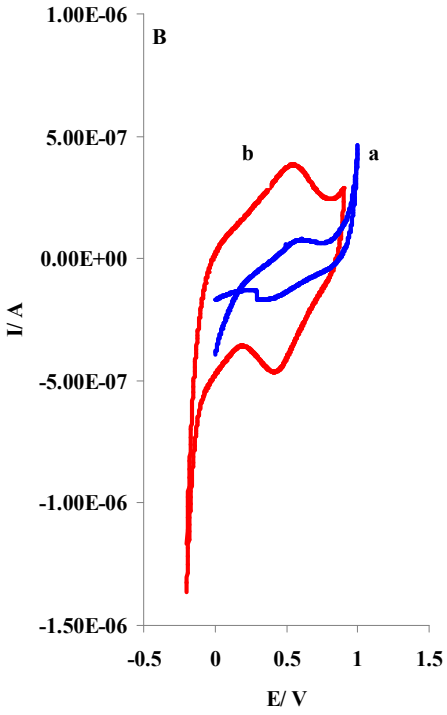

View Article Online
DOI: 10.1039/C3RA42393J

Magnetic nanoparticles loaded on mobile crystalline material-41: Preparation, Characterization and application as a novel material for construction electrochemical nanosensor

Mohammad Hasanzadeh [a*], Arash Bahrami [b], Mohammad Alizadeh [b*], Nasrin Shadjou [c]

[a] *Drug Applied Research Center, Tabriz University of Medical Sciences, Tabriz 51664, Iran.*

[b] *Department of Food Science and Technology, faculty of Health and Nutrition, Tabriz University of Medical Sciences, Tabriz, Iran.*

[c] *Biochemistry Lab, Pasteur Institute of Iran, Tehran, Iran.*

Corresponding author, E-mail address:
***** *mhmmd_hasanzadeh@yahoo.com, malizadeh@tbzmed.ac.ir*
Tel.: +98 461 2344384; fax: +98 461 2332556.

View Article Online
DOI: 10.1039/C3RA42393J

Abstract

Herein, we envisage the possibility of preparing stable magnetic mobile crystalline material-41 using cetyltrimethylammonium bromide and Fe_3O_4 nanoparticles. The Fe_3O_4 nanoparticles are incorporated into mobile crystalline material-41 in hydrothermal conditions. The prepared mesoporous sample was characterized by Fourier transform infrared spectrometry (FT-IR), X-ray diffraction (XRD), scanning electron microscopy (SEM) and nitrogen adsorption-desorption techniques. The electrochemical behavior of cadaverine, histamine and putrescine was investigated on magnetic mobile crystalline material-41 (MCM-41-Fe_2O_3) modified carbon past electrodes (CPE). Due to the very large surface area (1213 m^2 g^{-1}) and remarkable electrocatalytic properties of Fe_2O_3 nanoparticles, the MCM-41-Fe_2O_3 exhibits potent electrocatalytic activity toward the electro-oxidation of some selected biogenic amines. MCM-41-Fe_2O_3-CPE brings new capabilities for electrochemical sensing by combining the advantages of Fe_2O_3 magnetic nanoparticles and MCM-41 with very large surface area. The process of oxidation and its kinetics were established by using cyclic voltammetry, chronoamperometry techniques and also steady state polarization measurements. The apparent electron transfer rate constant (K_s) and transfer coefficient (α) were determined by cyclic voltammetry and were approximately 6.2 s^{-1} and 0.48, respectively. The linear concentration range of the proposed sensor for the cadaverine, histamine and putrescine were 0.1-10, 0.01-0.5 and 0.9-35 μM, respectively. Finally, the applicability of the sensor for determination of electroactive biogenic amine in fish samples has been successfully demonstrated.

Keywords: biogenic amine, electrocatalysis, mesoporous, kinetics, nanosensor.

View Article Online
DOI: 10.1039/C3RA42393J

1. Introduction

Recently, mesoporous molecular sieves have attracted significant attention in the field of adsorption, catalysis, and separation as they exhibit excellent characteristics such as a high surface area up to 1500 m^2 g^{-1}, a large pore volume, and a narrow pore size distribution between 2 and 15 nm. [1-4] Furthermore, using of mesoporous molecular as catalyst has attracted considerable interest in organic transformations, because of their high surface area-to-volume ratios. [5, 6] However, this small magnetic display low thermal stability and an affinity to form large agglomerate. [7] Moreover, their separation from the system for recycling remains a major complication in industrial application. [8]

Fe_2O_3 is a technologically important compound widely used for the production of magnetic materials and catalysts. Protection of the bare Fe_3O_4 is essential because they easily oxidize or dissolve in an acid medium during the treatment procedure. Silica is one of the best neutral coating layers for Fe_2O_3 due to its high chemical and thermal stability, large surface area and good compatibility. [9]

Biogenic amines are low-molecular-mass aliphatic, alicyclic and heterocyclic organic compounds displaying biological activity. They may be found in a wide range of food products of both animal and plant origin, as well as in fermented foods. They are produced mainly by the microbial decarboxylation of amino acids, in particular of the amino acid histidine. It is important to monitor biogenic amine levels in food stuffs and beverages in view of their importance for human health and food safety. Biogenic amines occasionally cause food poisoning in man. The most frequent kind of poisoning due to the histamine is known as “scombroid fish poisoning”, linked to consumption of fish like tuna and sardines, which contain high levels of histamine. [10-14]

View Article Online
DOI: 10.1039/C3RA42393J

Electrochemical sensors has a well-defined role in biological molecules, and various electroanalytical methods have attracted more attentions because of quick response, high sensitivity, abilities to miniaturization, and analysis of amines [15-18]. Because the detection of biogenic amines is very important, the trace determination of these molecules is of considerable importance in food chemistry. Electrochemical methods have been widely used for detection of these biological molecules. However, the detection limits are not low enough. Therefore, in the current study, an excellent electrochemical sensor based on MCM-41-Fe_2O_3 was constructed for the determination of selected biogenic amines. In this work, at continuation of our studies on application of mesoporous materials for the detection of amines [17, 18], an electrochemical analysis for biogenic amines was proposed by cyclic voltammetry (CV), differential pulse voltammetry (DPV) and chronoamperometry methods at a carbon paste electrode modified by magnetic MCM-41-Fe_2O_3 [MCM-41-Fe_2O_3-CPE]. As far as we are aware, there is no report on preparation of MCM-41-Fe_2O_3-CPE. Therefore, we constructed a new magnetic nanosensor for detection of electroactive biogenic amines in fish samples.

2. Experimental

Electrochemical experiments were performed with a computer-controlled Autolab modular electrochemical system (Eco Chemie Ultecht, The Netherlands), driven with GPES software (Eco Chemie). A conventional three-electrode cell was used with an SCE (Methrom, The Netherlands) as a reference electrode and a Pt wire as a counter-electrode. The working electrode was carbon paste electrode (CPE) electrode (Φ=2 mm) modified with MCM-41-Fe_2O_3 nanostructures. All measurements were conducted in a thermostated temperature of 20±1 °C. All chemicals used were of analytical grade from

View Article Online
DOI: 10.1039/C3RA42393J

Merck (Darmstadt, Germany) and were used without further purification. Briton Robinson buffers were prepared by initially dissolving 10 mL concentrated orthophosphoric acid, 8.7mL glacial acetic acid and 9.27g boric acid in water and diluting to 1.0L in a volumetric flask. This solution was subsequently used to prepare appropriate buffers by addition of 7.5M NaOH to reach the desired pH value. Voltammetric experiments on cadaverine, histamine and putrescine were carried out in 0.15M Briton Robinson buffer of pH 6.2.

The surface morphology of the modified electrodes was evaluated with a Vega-Tescan scanning electron microscope (SEM). X-ray diffraction (XRD) measurements were performed using a Philips diffractometer manufactured by X'pert with monochromatized CuKa radiation.

Cadaverine, Histamine, and Putrescine (were purchased as hydrochloride salts from Sigma (USA). Dansyl chloride for dansylation was obtained from Sigma Aldrich (Switzerland).

2.1. Standards

Stock solutions of the three biogenic amines were prepared separately to concentrations of 1 mg/ml in 0.1 M hydrochloric acid (HCl). A working solution was prepared by diluting 1 ml of each stock solution in 0.1 M HCl to a final volume of 10 ml. The Dansyl chloride solution (5 mg/ml) was prepared by dissolving 500 mg of Dansyl chloride in 100 ml of acetone. All solutions were kept at a temperature of 4 $^{\circ}$C prior to use.

2.2. Extraction

Biogenic amines extraction from the samples was carried out according to the procedures developed by Mah et al. [19] with a little modification. A 3g slurry of each sample was

View Article Online
DOI: 10.1039/C3RA42393J

transferred into a centrifuge tube containing 10 ml of 5% (w/v) trichloroacetic acid (TCA) and 200 µl of 1,7-diaminoheptane. The mixture was vortexed for 15 min and then centrifuged at 5000 g for 10 min at 4 $^{\circ}$C. The supernatant was collected and the residue was extracted again with the same volume of TCA. Both supernatants were filtered through Whatman paper No. 1 and combined. The final volume was adjusted to 25 ml with TCA.

2.3. Synthesis of MCM-41-Fe_2O_3

At first, MCM-41 was synthesized according to the previously described method using cetyltrimethylammonium bromide (CTMAB), as the templating agent. [20] Naked Fe_3O_4 were prepared from a solution with molar composition of 3.2 $FeCl_3$:1.6 $FeCl_2$:1 CTABr: 39 NH_4OH:2300 H_2O at room temperature. Typically, 2g of iron(III) chloride ($FeCl_3$. $6H_2O$) and 0.8 g of iron(II) chloride ($FeCl_2$. $4H_2O$) were dissolved in 10 mL of distilled water under N_2 atmosphere. The resulting solution was added dropwise to a 100 mL solution of 1.0 M NH_4OH solution containing 0.4g of cetyltrimethylammonium bromide (CTAB) to produce a colloidal suspension of iron oxide magnetic. The magnetic MCM-41 was prepared by adding 20 mL of the magnetic colloid to a 1L solution with the molar composition of 292 NH_4OH:1CTAB:2773 H_2O under vigorous mixing and sonication. Then sodium silicate was added, and the mixture was allowed to react at room temperature for 24 h under well-mixed conditions. The magnetic MCM-41 was filtered and washed. The surfactant template was then removed from the synthesized material by calcination at 450^{o}C for 3h (Scheme 1). MCM-41-Fe_2O_3 was characterized with Fourier transform infrared spectrometry (FT-IR), scanning electron microscope (SEM). X-ray diffraction (XRD) and Transmission electron microscopy (TEM) (Fig. 1). The SEM and

View Article Online
DOI: 10.1039/C3RA42393J

the TEM showed that the encapsulated were present as uniform particles and the size of encapsulated was about 34 nm (Fig. 1A, B).

At IR spectra the band from 400-650 cm^{-1} is assigned to the stretching vibrations of (Fe-O) band in Fe_2O_3, and the band at about 1100 cm^{-1} is ascribed to stretch of (Si-O) bond.

The XRD analysis was performed from 1.0° (2θ) to 10.0° (2θ) (Fig. 1C). The XRD patterns of the synthesized catalyst are presented in Fig. 1D. The sample of MCM-41-Fe_2O_3 showed relatively well-defined XRD patterns, with one major peak along with one small peak identical to those of MCM-41 materials.

The N_2 adsorption isotherms after embedded of Fe_2O_3 were recorded and shown in Fig. 2. The specific surface area and total pore volume obtained by the N_2 adsorption isotherms and calculated by the Brunauer-Emmett-Teller (BET) method [21] were 1213 m^2 g^{-1} and 1.59 cm^3 g^{-1}, respectively. The pore diameter of the MCM-4-Fe_2O_3 was 5.26 nm derived from the adsorption and desorption branches by the Broekhoff and deBoer model. [21]

It is important to note that the magnetic property of this catalyst facilitates its efficient recovery from the reaction mixture during work-up procedure. In the presence of an external magnet, recoverable MCM-41-Fe_2O_3 moved onto the magnet steadily and the reaction mixture turned clear within 10 s (Fig. 3).

2.4. Preparation of modified MCM-41-Fe_2O_3 electrodes

The unmodified carbon-paste electrode was prepared by mixing graphite powder with appropriate amount of mineral oil (Nojol) and thorough hand mixing in a mortar and pestle (60:25, w/w,(and a portion of the composite mixture was packed into the end of a polyethylene syringe (2.5 mm diameter). Electrical contact was made by forcing a thin copper wire down into the syringe and into the back of the composite. The modified

View Article Online
DOI: 10.1039/C3RA42393J

electrode was prepared by mixing unmodified composite with MCM-41-Fe_2O_3 (15%, w/w). Then, the modified composite was packed into the end of a polyethylene syringe.

3. Results and discussion

Results of previous works showed that the CPEs modified with various types of nano-particles have catalytic effects in the electro-oxidation of biological molecules. The catalytic rule of the modifier causes enhancement of the anodic peak current in the electrode process. Fig. 4 shows cyclic voltammograms of 0.15M Briton Robinson buffer (pH 6.2) solution recorded using unmodified electrode (UCPE)(A) and MCM-41-Fe_2O_3 modified electrode (MCM-41-Fe_2O_3-CPE) (B) in the absence (curves a) and presence (curves b) of 10μM histamine in the potential range of 0 to 1V. Histamine represents very weak oxidation signal on UCPE. On the other hand, histamine was oxidized on MCM-41-Fe_2O_3-CPE surface via a single anodic peak located at around 0.53 V. In addition, the anodic current densities related to the electrooxidation of the histamine on the MCM-41-Fe_2O_3-CPE surface. In the entire range of potential window of aqueous electrolytes, different Fe species are created, and the Fe (II)/Fe (III) redox transition performs at the anodic edge of the voltammograms. Fe species are immobilized on the electrode surfaces, and the one with a higher valence oxidizes histamine *via* chemical reactions. Fe(II) species can oxidize organic and biological compounds by chemical reaction(s) between organic and biological compounds and Fe(II) species *via* a redox mediation electron transfer process (mediated electrocatalytic reaction, EC′ mechanism). The results indicated that histamine was oxidized by an active Fe (III) moiety through a cyclic mediation redox process. Higher-valence iron (Fe (III) species) oxidized histamine *via* a chemical reaction followed by the generation of low-valence iron (Fe (II) species).

View Article Online
DOI: 10.1039/C3RA42393J

Similarly, the high-valence oxide is regenerated through the external electrical circuit. Accordingly, histamine is oxidized *via* an EC′ mechanism. Therefore, the electrode reactions may proceed *via* a mechanism involving a rate-limiting step, in which product species are formed upon chemical reactions of histamine with Fe (II) species, and regeneration of the surface occurs through chemical redox reactions. The participation of Fe(II) species as the catalyst of the electrooxidation reaction and the dominated EC' mechanism is further supported by the variation of current function (peak current divided by the square root of the potential sweep rate) with respect to the square root of the potential sweep rate. The data for these variations which were obtained from cyclic voltammograms recorded at different potential sweep rates are represented in Fig. 4C. In this figure, current function is smoothly decreased upon increasing the potential sweep rate confirming the electrocatalytic nature of the electrooxidation process. Based on the represented explanation and the results, the following mechanism can be proposed for the mediated oxidation of on the MCM-41-Fe_2O_3-CPE surface. The redox transition of the iron species:

$$Fe^{II} \underset{k-1}{\overset{k_1}{\rightleftharpoons}} Fe^{III} + e \qquad (2)$$

is followed by the oxidation of histamine on the MCM-41-Fe_2O_3-CPE surface in two steps via the following reactions:

$$Fe^{III} + \text{histamine} \xrightarrow{k_2(E)} intermediate + Fe^{II} \qquad (3)$$

$$Fe^{III} + intermediate \xrightarrow{k_3(E)} product + Fe^{II} \qquad (4)$$

On the other hand, generally, metal catalysts have been used to increase the sensitivity of proposed sensor. The first step in every heterogeneous catalytic reaction is the adsorption of reacting species biogenic amines on the active phase of the catalyst (MCM-41-Fe_2O_3). There intra molecular bonds are broken or weakened. Subsequently the adsorbed species

View Article Online
DOI: 10.1039/C3RA42393J

react with the surface of films. This generally occurs in consecutive steps until the desired product is reached which desorbs afterwards (Scheme 2).

The oxidation process of the MCM-41-Fe_2O_3 exhibited high electrocatalytic responses for histamine, cadaverine and putrescine, therefore, demonstrating its exhibiting capability for selective oxidation of selected biogenic amines. For further confirmation, all mechanisms for the studied biogenic amines are presented in Scheme 3.

The proposition of a one-step reaction for the electrocatalytic oxidation of histamine on the MCM-41-Fe_2O_3-CPE surface (reactions 2 and 3) is based on the appearance of one anodic peak in the corresponding voltammogram (Fig.4B, curve b). Higher catalytic rate of the electrooxidation reaction can be related to nanometer dimension of MCM-41-Fe_2O_3. The MCM-41-Fe_2O_3 is stably distributed on the electrode surface which is fully and easily accessible histamine and, consequently, can be readily and completely used as electrochemical reaction units. Moreover, MCM-41-Fe_2O_3 are often irregularly shaped objects, and hence, there are some defect sites, such as steps that separate planar atomic terraces or kinks where a step advances or recedes, exposing corner or edge atoms on a plane. The enhancement of the reactivity of these defective sites can be so large that their presence determines to a very large extent the catalytic activity of MCM-41-Fe_2O_3. Similar cyclic voltammograms were recorded for cadaverine and putrescine (Figs. 5A and B).

Fig. 6A displays typical cyclic voltammograms for MCM-41-Fe_2O_3-CPE in a buffer solution (pH 6.2) at different scan rates. Figs. 6 A and B show that the anodic peak currents are directly proportional to the scan rate of the potential at a sweep rate from 5-700 s^{-1}. The plot of peak current *versus* the scan rate up to 20 mV s^{-1} had good linearity as

View Article Online
DOI: 10.1039/C3RA42393J

expected for surface confined redox processes. The small peak-to-peak separation and good linearity between the peak currents and scan rates at sweep rates of 5-700 mV s^{-1} suggested facile charge transfer kinetics. At higher scan rates, the peak currents *vs.* scan rate plots deviated from linearity and the peak currents became proportional to the square root of the potential scan rate. The data indicated that the peak current was diffusion controlled. In addition, with increasing scan rates, the peak separations began to increase, indicating that the limitation arose from charge transfer kinetics. Based on Laviron theory, [22] the electron transfer rate constant (K_s) and charge transfer coefficient (α) could be determined by measuring the variation of peak potential with scan rate. The peak potential values were proportional to the logarithm of the scan rate for the rates higher than 20mV s^{-1} (Fig. 6C). The calculated values for (K_s) and (α) were approximately 6.2 s^{-1} and 0.48, respectively. The surface concentration of electroactive species (Γ) can be calculated from the slope of the plot of I_{pa} verses scan rate and is about 3.71 $\times 10^{-9}$ mole cm^2.

In order to evaluate the reaction kinetics, the oxidation of these biogenic amines on MCM-41-Fe_2O_3-CPE was investigated by chronoamperometry. Chronoamperometry, as well as cyclic voltammetry has been employed for the investigation of the processes occurring *via* an E_rC_i mechanism. [22] Single steps chronoamperograms were recorded by setting the working electrode potentials to desired values and were used to measure the catalytic rate constant on the modified surface. Fig. 7A shows single steps chronoamperograms for the modified electrode in the absence (a) and presence (b: 0.01, c: 0.03, d: 0.05, e: 0.08, f: 0.1 and g: 0.5 μM of histamine over a concentration range of 0.01-0.5 μM. The applied potential step was 0.53V. The plot of net current versus $t^{-1/2}$

View Article Online
DOI: 10.1039/C3RA42393J

which has been obtained by removing the background current by the point-by-point subtraction method gives a straight line, Fig. 7B. This indicates that the transient current must be controlled by a diffusion process. By using the slopes of these lines; we can obtain the diffusion coefficients of the histamine according to the Cottrell equation: [23]

$$I = nFAD^{1/2}C^{*}\pi^{-1/2}t^{-1/2} \quad (5)$$

where D is the diffusion coefficient, and C^{*} is the bulk concentration. The mean value of the diffusion coefficients of histamine was found to be 3.30×10^{-5} cm^2 s^{-1}.

The rate constants of the reactions of histamine and the ensuing intermediates with the redox sites of the MCM-41-Fe_2O_3-CPE can be derived from the chronoamperograms according to Eq. (6): [23]

$$\frac{I_{catal}}{I_d} = \lambda^{1/2}\left[\pi^{1/2}erf(\lambda^{1/2}) + \frac{\exp(-\lambda)}{\lambda^{1/2}}\right] \quad (6)$$

where I_{catal} is the catalytic current in the presence of histamine , I_d the limiting current in the absence of histamine and $\lambda=kC_mt$ (k, C_m and t are the catalytic rate constant, bulk concentration of histamine and the elapsed time, respectively) is the argument of the error function. For $\lambda > 1.5$, $erf(\lambda^{1/2})$ almost equals unity and Eq. (6) reduces to:

$$\frac{I_{catal}}{I_d} = \lambda^{1/2}\pi^{1/2} = \pi^{1/2}(kC_mt)^{1/2} \quad (7)$$

From the slope of the I_{catal}/I_d plot the value of k at a given concentration of histamine can be derived (Fig. 7C). The mean value of k in the concentration range of 0.01-0.5 μM histamine was found to be $2\times10^{+6}$ cm^3 mol^{-1} s^{-1}. It should be pointed out that k is either k_2 or k_3 whichever is smaller. Similar chronoamperograms were collected for cadaverine and putrescine. The values of D and k obtained according to the method described in the above for these biogenic amines were reported in Table 1.

View Article Online
DOI: 10.1039/C3RA42393J

The rate laws for the reactions 3 and 4 have the forms of:

$$\nu_1 = k_1 \Gamma \theta_{II} - k_{-1} \Gamma \theta_{III} \quad (8)$$

$$\nu_2 = k_2 \Gamma \theta_{III} C_m \quad (9)$$

where Γ is the total number of adsorption sites per unit area of the electrode surface, θ represents the fractional surface coverages of different iron valence states and C_m is the bulk concentration of histamine. With only the 2 and 3 valence states of iron prevailing one has:

$$\theta_{II} + \theta_{III} = 1 \quad (10)$$

and the rates of changes of their surface coverages as well as those of the intermediate compounds are:

$$\frac{d\theta_{II}}{dt} = -\frac{d\theta_{III}}{dt} = -k_1 \theta_{II} + k_{-1} \theta_{III} + k_2 \theta_{III} C_m + k_3 \theta_{III} C_i \quad (11)$$

$$\frac{dC_i}{dt} = k_2 \theta_{III} C_m - k_3 \theta_{III} C_i \quad (12)$$

where C_i is the concentration of the intermediate. Assuming that the steady state dominates:

$$\frac{d\theta_{II}}{dt} = -\frac{d\theta_{III}}{dt} = 0 \quad (13)$$

$$\frac{dC_i}{dt} = 0 \quad (14)$$

one arrives at the values if the coverages:

$$\theta_{II} = \left(\frac{k_{-1} + 2k_2 C_m}{k_1 + k_{-1} + 2k_2 C_m} \right) \quad (15)$$

$$\theta_{III} = \left(\frac{k_1}{k_1 + k_{-1} + 2k_2 C_m} \right) \quad (16)$$

View Article Online
DOI: 10.1039/C3RA42393J

and subsequently:

$$\nu_1 = \left(\frac{2k_1 \Gamma k_2 C_m}{k_1 + k_{-1} + 2k_2 C_m} \right) \tag{17}$$

on the basis of this rate equation the faradic current will be:

$$i_f = \left(\frac{2FAk_1 \Gamma k_2 C_m}{k_1 + k_{-1} + 2k_2 C_m} \right) \tag{18}$$

where A is the surface area of the electrode and the rate constants k_1 and k_{-1} are obviously potential dependent and are of the forms:

$$k_1(E) = k^0{}_1 \exp\left[\frac{\alpha nFE}{RT} \right] \tag{19}$$

$$k_{-1}(E) = k^0{}_{-1} \exp\left[\frac{(\alpha - 1)nFE}{RT} \right] \tag{20}$$

where k_{-1}° and k_1° are the chemical rate constants measured at E *vs.* (Ag/AgCl)/V = 0 with a being the anodic transfer coefficient and other parameters have their usual meanings. Equation (20) is well suited for the calculation of rate constants and the validity test of the kinetics and mechanism of the oxidation process.

The pseudo-steady state polarization curves of the electro-oxidation of histamine on the MCM-41-Fe_2O_3-CPE at a number of histamine concentrations are presented in Fig. 8. The oxidation process was found to begin at nearly 0.35V and to reach a plateau at 0.78V while the oxygen evolution started at still higher potentials. In the course of reaction the coverage of MCM-41-Fe_2O_3 increases and reaches a saturation (steady state) level and the oxidation current follows accordingly. According to Eq. (20) the plots of the inverse of current against the inverse of histamine concentration should be linear:

View Article Online
DOI: 10.1039/C3RA42393J

$$i_f^{-1} = (FAk_1\Gamma)^{-1} + \left[\frac{k_1 + k_{-1}}{2FAk_1k_2\Gamma}\right] C_m^{-1} \quad (21)$$

Fig. 9A presents the i^{-1} versus C_m^{-1} dependency where straight lines at various potentials have been obtained. Both the intercepts and slopes of the straight lines appearing in this figure were potential dependent. The slopes are plotted against *exp (–nFE/RT)* with n =1 and the graph is presented in Fig. 9B. Using this graph along with Eq. (21) reveals that the rate constant of reaction 5, $k_2\Gamma$ and the ratio of k^o_{-1}/k^o_1 are 3.09×10^{-8} cm s^{-1} and $5.00\times10^{+10}$, respectively. Fig. 9C presents the variation of the intercepts of the lines in Fig. 8B with the applied potential on a semi-log scale.

Using this graph and Eq. (21) the magnitudes of $k^o_1\Gamma$ and the anodic transfer coefficient of 8.66×10^{-10} mol s^{-1} cm^{-2} and 0.48 have been obtained. From the above findings the value of $k^o_{-1}\Gamma$ was worked out to be 7.20×10^{1} mol s^{-1} cm^{-2}. Similar pseudo-steady state polarization curves were collected for cadaverine and putrescine.

The dependence of histamine concentration on $(di_f/dE)^{-1}$ is illustrated in Fig. 9D where the initial sharp drops flatten out to a very slow change as the concentrations of histamine increase. The results are further fitted to Eq. (22):

$$\left(\frac{di_f}{dE}\right)^{-1} = \frac{(k_1 + k_{-1} + 2k'C_{\text{histamine}})^2}{\left[\dfrac{2FA\Gamma k'C_{\text{histamine}}\, k_1(2\alpha Fk'C_{\text{histamine}})}{RT + (\dfrac{k_{-1}F}{RT})}\right]} \quad (22)$$

to estimate the values of the rate constants. From the fitted equation (with regression equations of $y = (6.56\times10^{3}x^2 + 2.30\times10^{-1}x + 5.45\times10^{-3})/(1.10\times10^{2}x^2 + 2.50\times10^{-1}x)$ with $R^2 = 0.9950$ for histamine and using the corresponding value of α obtained above, the mean values of the rate constants for iron redox transition were obtained as k^o_1=6.2 s^{-1}

View Article Online
DOI: 10.1039/C3RA42393J

and k^o_{-1}=1.25×10^{-2} s^{-1}. Also, the value of the catalytic rate constant and the maximum of surface concentration of adsorption sites were obtained as k'= 4.00×10^{+5} L mol^{-1} s^{-1} and Γ= 3.71 ×10^{-9} mol cm^{-2}. The values of k^o_{-1}, k^o_1, α obtained according to the method described in the above for three biogenic amines were reported in Table 2.

The calibration curve for histamine concentration in 0.15M Briton Robinson buffer of pH 6.2 solution was obtained by differential pulse voltammetry (DPV). Fig. 10A shows typical DPV curves for different concentrations of histamine in buffer solution. The dependency between peak current and histamine concentration was rectilinear within the range of 0.01 to 0.5μM (with a regression equation of y = 47.46x + 74.71, R^2 = 0.9993, n=5), Fig. 10B. The limits of detection (LOD) and quantification (LOQ) of the procedure were calculated according to the 3 S.D/m criteria where S.D. is the standard deviation of the blank and m is the slope of the calibration curves.[24] The limits of detection and quantification were found to be 0.003 μM and 0.007μM. Precision and accuracy were assessed by performing replicate analyses of histamine samples. The precision of the method was calculated as the relative standard deviation (RSD). The procedure was repeated on the same day on the same solutions at concentrations in the range of the standard series. The intra-assay RSDs of the proposed method determined on the basis of peak current for 6 replicates, was (4.10%), and showed good repeatability. Similar DPV curves were collected for cadaverine and putrescine. The values of LOD (μM), LOQ (μM) and linear range (μM) obtained according to the method described for three biogenic amines were reported in Table 3.

The high sensitivity of the method allows the determination of histamine, cadaverine and putrescine in spiked fish samples. The recovery of the analytes was measured by spiked

View Article Online
DOI: 10.1039/C3RA42393J

into highly diluted fish samples. The differential pulse voltammograms were recorded after the fish samples was spiked with various amounts of the biogenic amines within the working concentration rang. Recoveries were found to lie in rang of 93 to 106%. The results are listed in Table 4.

4. Conclusion

MCM-41-Fe_2O_3 have been employed to modification of carbon paste electrode and used as an efficient nanosensor for the electrocatalytic oxidation of histamine, cadaverine and putrescine in Briton Robinson buffer. The modified electrodes showed excellent electrocatalytic potential for the oxidation of various histamine, cadaverine and putrescine at a remarkably positive potential in alkaline solutions. The micromolar concentrations of these analytes were determined by a differential pulse voltametry method at the surface of the modified electrode. The simple preparation procedure, reproducibility, high stability, wide linear range, low detection limit, distinct advantage of polishing in the event of surface fouling suggest that the prepared modified electrode can be used as a chronoamperometric detector for biogenic amines determination in flow systems or in chromatographic instruments.

Acknowledgements

We gratefully acknowledge the partial support of this work by Nutritional research center, Tabriz University of Medical Sciences.

View Article Online
DOI: 10.1039/C3RA42393J

5. References

1. J. Deutsch, H.A. Prescott, D. Muller, E. Kemnitz, *J. Catal.,* 2005, ***231***, 269-278.

2. D. Zhao, Q. Huo, J. Feng, B.F. Chmelka, G.D. Stucky, *J. Am. Chem. Soc.,* 1998, ***120***, 6024- 6036.

3. W. Zhang, T.R. Pauly, T. Pinnavaia, *J. Chem. Mater.,* 1997, ***9***, 2491- 2498.

4. A. Galarneau, D. Desplantier-Giscard, F. Di Renzo, F. Fajula, *Catal. Today* 2001, ***68***, 191-200.

5. V.Y. Gusev, X. Feng, Z. Bu, G.L. Haller, J.A. O'brien, *J. Phys. Chem.,* 1996, ***100***, 17725-17731.

6. F. Hoffmann, M. Cornelius, J. Morell, M. Fröba, *Angew. Chem. Int. Ed.,* 2006, ***45***, 3216-3251.

7. X. Wang, S. Cheng, *Catal. Commun.,* 2006, ***7***, 689-695.

8 D. Macquarrie, D. Jackson, *Chem. Commun.,* 1997, 1761-1762.

9. M. Hasanzadeh, N. Shadjou, M. de la Guardia, M. Eskandani, P. Sheikhzadeh, *Trends Anal. Chem.,* 2012, ***33***, 117-129.

10. L.F. Bjeldanes, D.E. Schutz, M.M. Morris, *Food Cosmet. Toxicol.,* 1978, ***16***, 157-159.

11. J.L. Parrot, M. Gabe, A. Herrault, *C. R. Soc. Biol. (Paris)* 1947, ***144***, 486.

12. J.L. Parrot, *C. R. Soc. Biol. (Paris)* 1948, ***142***, 631.

13. H.P. K Jung, L.F. Bjeldanes, *Food Cosmet. Toxicol.,* 1979, ***17***, 629-632.

14. S.L. Taylor, E.R. Lieber, *Food Cosmet. Toxicol.,* 1979, ***17***, 237-240.

15. Tanya Tsonkeva, 2001

16. Guo,H.-Talanta 2005,

View Article Online
DOI: 10.1039/C3RA42393J

17. M. Hasanzadeh, N. Shadjou, S.T. Chen, P. Sheikhzadeh, *Catal. Commun.,* 2012, ***19***, 21-27.

18. M. Hasanzadeh, N. Shadjou, E. Omidinia, P. Sheikhzadeh, *Colloids Surf. B: Biointerfaces,* 2013*,* ***108,*** 52-59.

19. H.K. Mah, J.H. Han, Y. J. Oh, M.G. Kim, H.J. Hwang, *Food Chem.,* 2002, ***79***, 239-243.

20. H. Takahashi, B. Li, T. Sasaki, C. Miyazaki, T. Kajino, S. Inagaki, *Micropor. Mesopor. Mater.* 2001, ***44-45***, 755-762.

21. P. Barrett, L.G. Joyner, P.H. Halenda, *J. Am. Chem. Soc.,* 1951, ***73***, 373-380.

22. E. Laviron, J. Electroanal. Chem. 1979, ***101***, 19-28.

23. A.J. Bard, L.R. Faulkner, Electrochemical Methods, Wiley, New York, 2001, Chapter 12

24. J.C. Miller, J.N. Miller, Statistics for Analytical Chemistry, fourth ed., Ellis Harwood, New York, 1994.

View Article Online
DOI: 10.1039/C3RA42393J

Figure Legends

Figure 1. The SEM and TEM (**A** and **B**) and **C and D**) FT-IR and XRD spectra of [MCM-41-Fe_2O_3], respectively.

Figure 2: (a) Nitrogen adsorption/desorption isotherm, (b) BJH of MCM-41-Fe_2O_3.

Figure 3: catalyst recovery at the reaction.

Figure 4: Cyclic voltammograms recorded in the absence (a) and presence of 10μM histamine (b) in 0.15M Briton Robinson buffer of pH 6.2 solution using UCPE (**A**) and MCM-41-Fe_2O_3-CPE (**B**). The potential sweep rate was 100mV s^{-1}. The insets show the derivative voltammograms (**C**) Variation of peak currents with the square root of the potential sweep rate.

Figure 5: (**A**) Cyclic voltammograms recorded in the absence (a) and presence of 10μM cadavarine (b) in 0.15M Briton Robinson buffer of pH 6.2 solution using MCM-41-Fe_2O_3-CPE. (**B**) Cyclic voltammograms recorded in the absence (a) and presence of 0.1mM putrescine (b) in 0.15M Briton Robinson buffer of pH 6.2 solution using MCM-41-Fe_2O_3-CPE. The insets show the variation of peak currents with the square root of the potential sweep rate.

Figure 6: (**A**) Cyclic voltammograms of the MCM-41-Fe_2O_3-CPE electrode in 0.15M Briton Robinson buffer of pH 6.2 solution in the presence of 10μM histamine various potential sweep rates of 5, 10, 20, 30, 40, 50, 75, 100, 150, 200,250, 300, 350, 400, 450, 500, 550, 600, 650, 700 mV s^{-1}. (**B**) Dependence of anodic peak current during the forward sweep on the square roots of potential sweep rate.

Figure 7: A: Double step chronoamperograms of the MCM-41-Fe_2O_3-CPEelectrode in the absence (a) and the presence of (b: 0.01, c: 0.03, d: 0.05, e: 0.08, f: 0.1 and g: 0.5 μM

View Article Online
DOI: 10.1039/C3RA42393J

histamine in 0.15M Briton Robinson buffer of pH 6.2 solution. Potential steps were 0.53V. **B**: Dependency of transient current on $t^{-1/2}$. **C**: Dependence of I_{catal}/I_d on $t^{1/2}$ derived from the data of chronoamperograms of (a) and (g) in main panel.

Figure 8: Typical pseudo-steady state polarization curves of MCM-41-Fe_2O_3-CPEelectrode obtained in 0.01(a), 0.1 (b), 1 (c) and 10 μM (d) histamine, respectively. The potential sweep rate is 0.005mV s^{-1}.

Figure 9: A: Plot of i^{-1} (from polarization curves in Fig.6) against C^{-1} at various potentials: 0.45, 0.47, 0.49, 0.5, 0.53, 0.55, 0.57 and 0.6 V as curves (a-h). **B**: Plot of the slopes (of curves in A) *vs.* Exp *(-nFE/RT*). **C**: Plot of the Ln (intercepts) (of curves in A) *vs.* applied potential. **D**: histamine concentration dependencies of $(di_f/dE)^{-1}$.

Figure 10: A: Differential pulse voltammograms obtained for determination of histamine 0.15M Briton Robinson buffer of pH 6.2 solution. Histamine concentrations from inner to outer are: 0.01, 0.03, 0.05, 0.07, 0.08, 0.09, 0.125, 0.15, 0.2, 0.25, 0.3, 0.4, and 0.5μM. **B**: The related calibration graph for concentration 0.01-0.5μM.

Scheme 1: Preparation of (α-Fe_2O_3)-MCM-41 nanocatalyst

Scheme 2: Graphic illustration of MCM-41-Fe_2O_3-CPE interaction

Scheme 3: Oxidation mechanism of **A**: cadaverine, **B**: histamine and **C**: putrescine.

View Article Online
DOI: 10.1039/C3RA42393J

Table 1: Values of the electrocatalytic reaction rate constants (k) and the diffusion coefficients (D) obtained from chronoamperometry curves

Analyte	D /cm^2 s^{-1}	k /cm^{3}mol^{-1}s^{-1}
cadaverine	7.75×10^{-5}	$3.67\times10^{+6}$
histamine	3.30×10^{-5}	$2.00\times10^{+6}$
putrescine	4.18×10^{-5}	$4.23\times10^{+6}$

Table 2: Values of the k^o_{-1}, k^o_1, α and b (Tafel slope) obtained from polarization curves.

Analyte	k^o_{-1}/s^{-1}	k^o_1/s^{-1}	α
cadaverine	1.00×10^{-2}	5.5	0.50
histamine	1.25×10^{-2}	6.2	0.48
putrescine	4.90×10^{-2}	7.1	0.50

Table 3: Results obtained from selected biogenic amines analysis in 0.15 M Briton Robinson buffer of pH 6.2 solution

Analyte	Linear range/µM	LOD/µM	LOQ/µM	RSD (%)
cadaverine	0.1-10	0.05	0.09	3.77
histamine	0.01-0.5	0.004	0.008	4.10
putrescine	0.9-35	0.06	0.1	2.85

Table 4: Recoveries of histamine, cadaverine and putrescine from spiked samples with MCM-41-Fe_2O_3-CPE

Analyte	Added /µM	Found [a]/µM	Recovery (%)
cadaverine	0	Not detected	-
	5	5.16	103.2
	10	9.47	94.7
	50	48.7	97.4
histamine	0	Not detected	-
	5	5.3	106.0
	10	10.28	102.8
	50	51.5	103.0
putrescine	0	Not detected	-
	5	5.00	100
	10	9.32	93.2
	50	49.0	98.0

[a] Average of six determinations at optimum conditions.

View Article Online
DOI: 10.1039/C3RA42393J

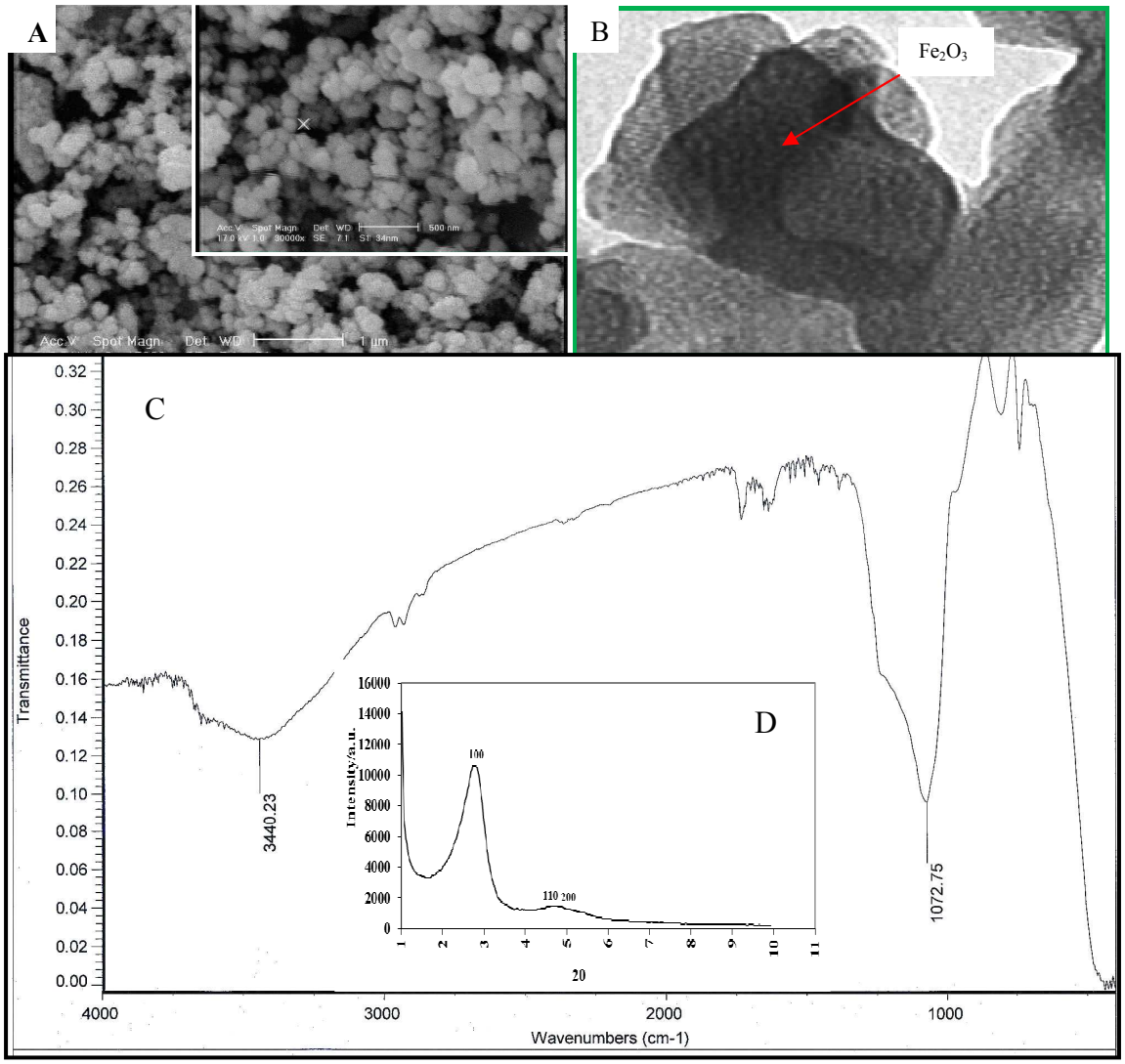

Fig. 1

View Article Online
DOI: 10.1039/C3RA42393J

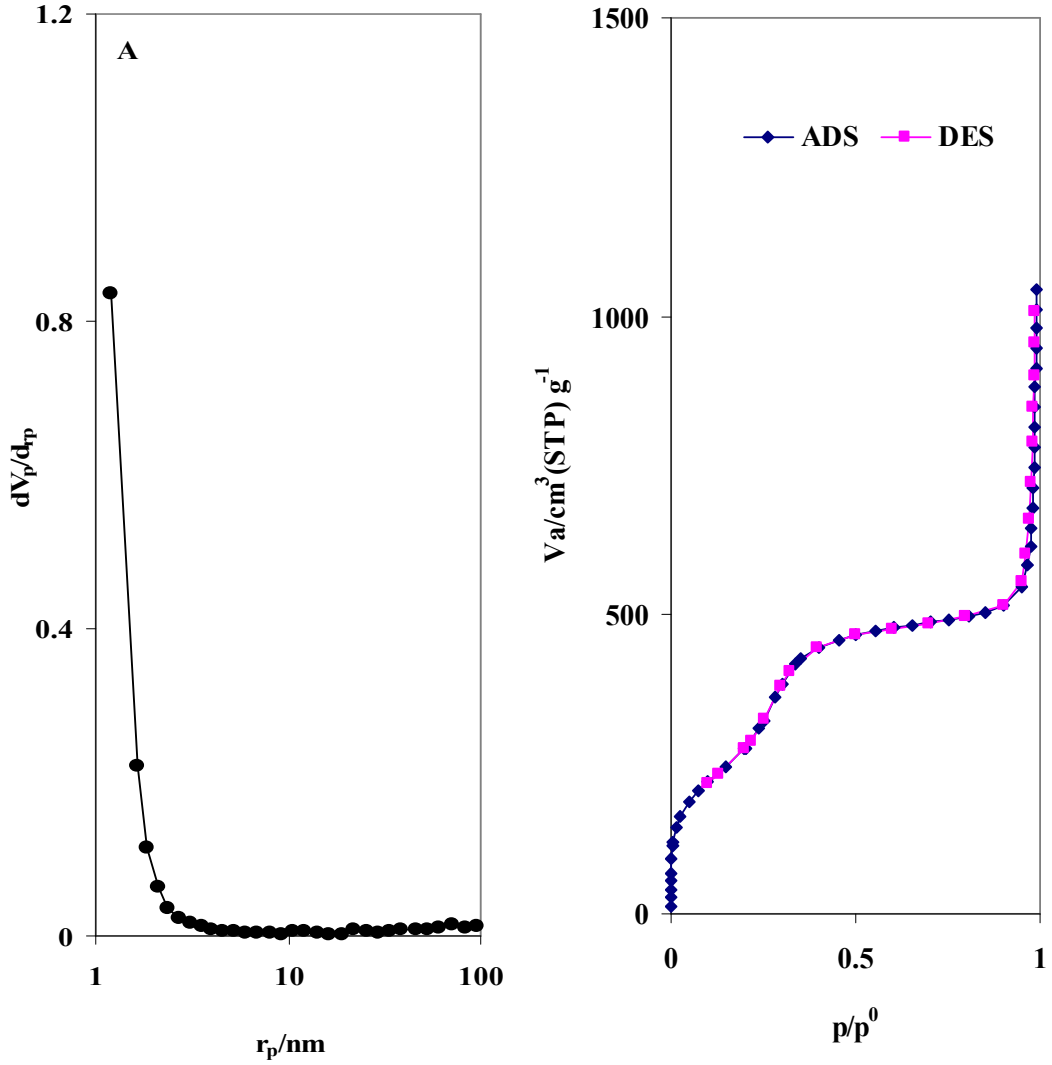

Fig. 2

View Article Online
DOI: 10.1039/C3RA42393J

Fig. 3

View Article Online
DOI: 10.1039/C3RA42393J

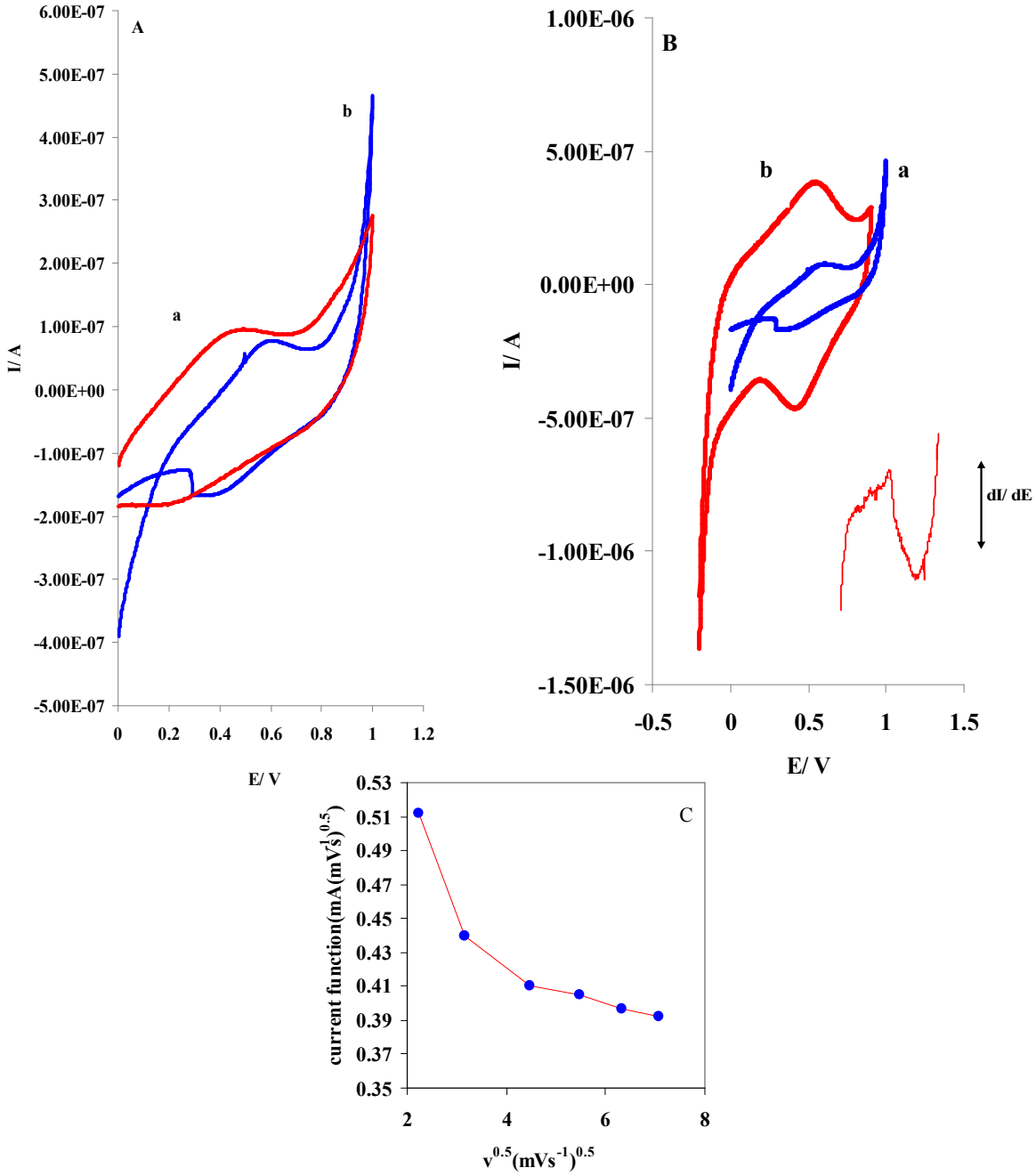

Fig. 4

View Article Online
DOI: 10.1039/C3RA42393J

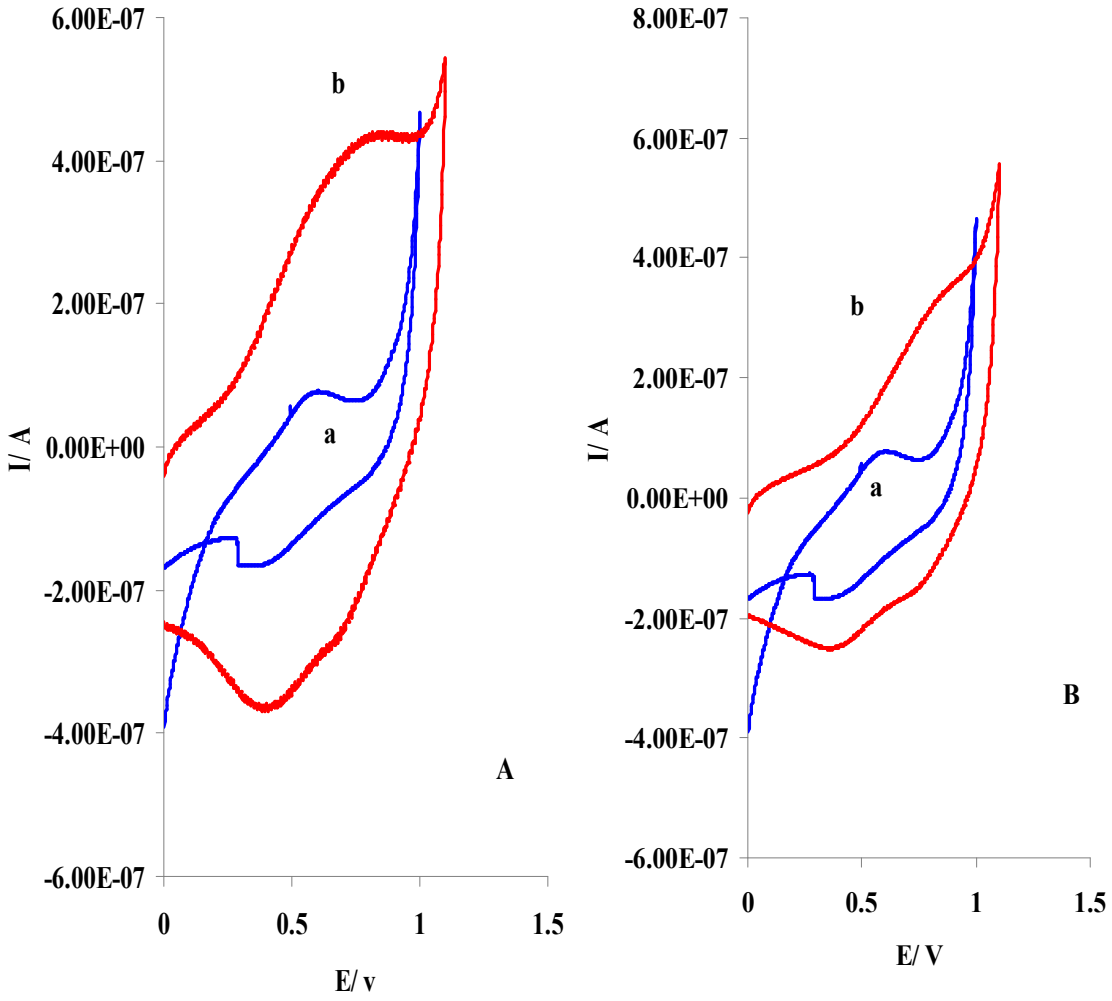

Fig. 5

View Article Online
DOI: 10.1039/C3RA42393J

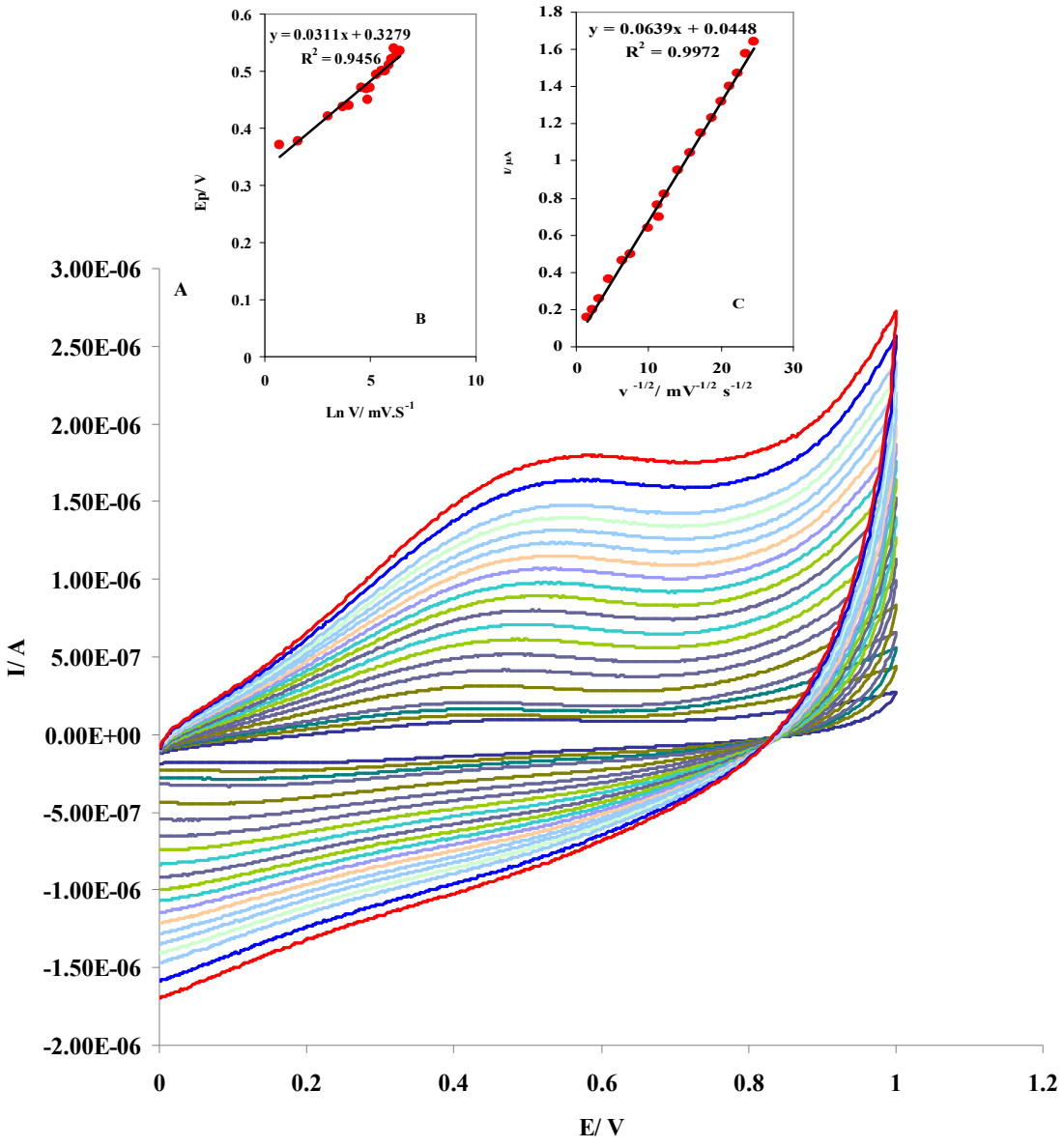

Fig. 6

View Article Online
DOI: 10.1039/C3RA42393J

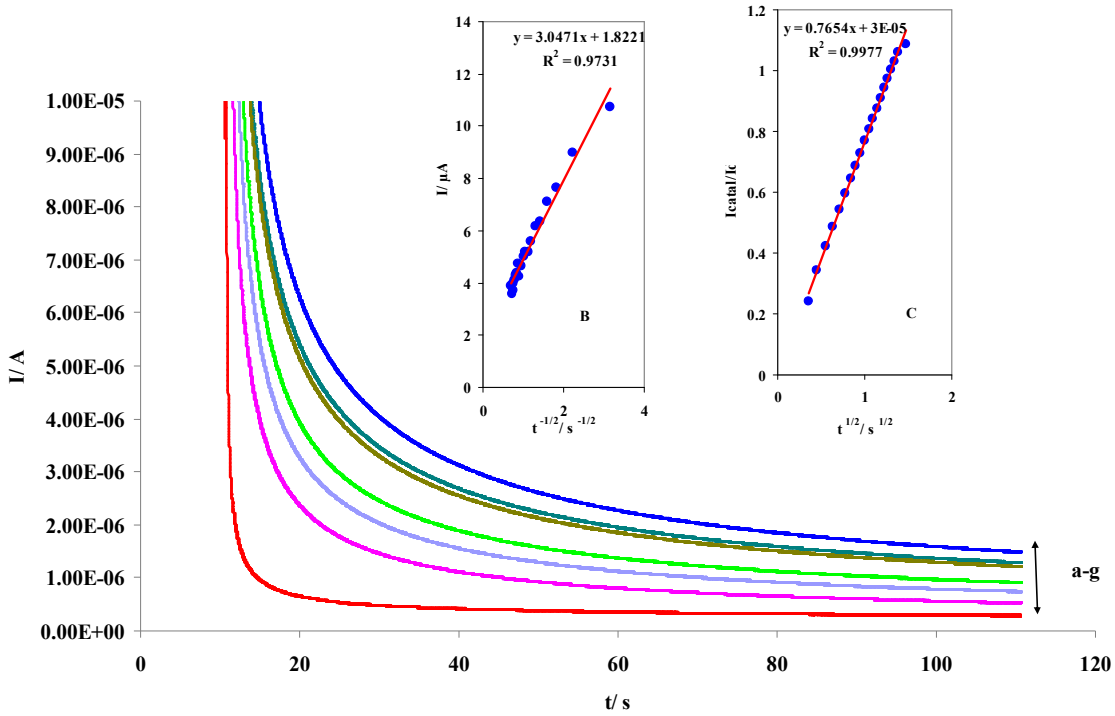

Fig. 7

View Article Online
DOI: 10.1039/C3RA42393J

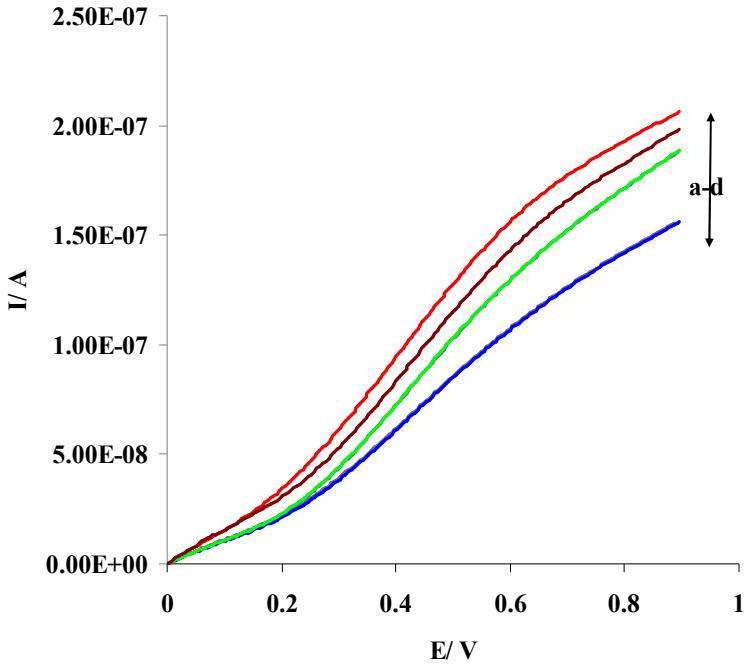

Fig. 8

View Article Online
DOI: 10.1039/C3RA42393J

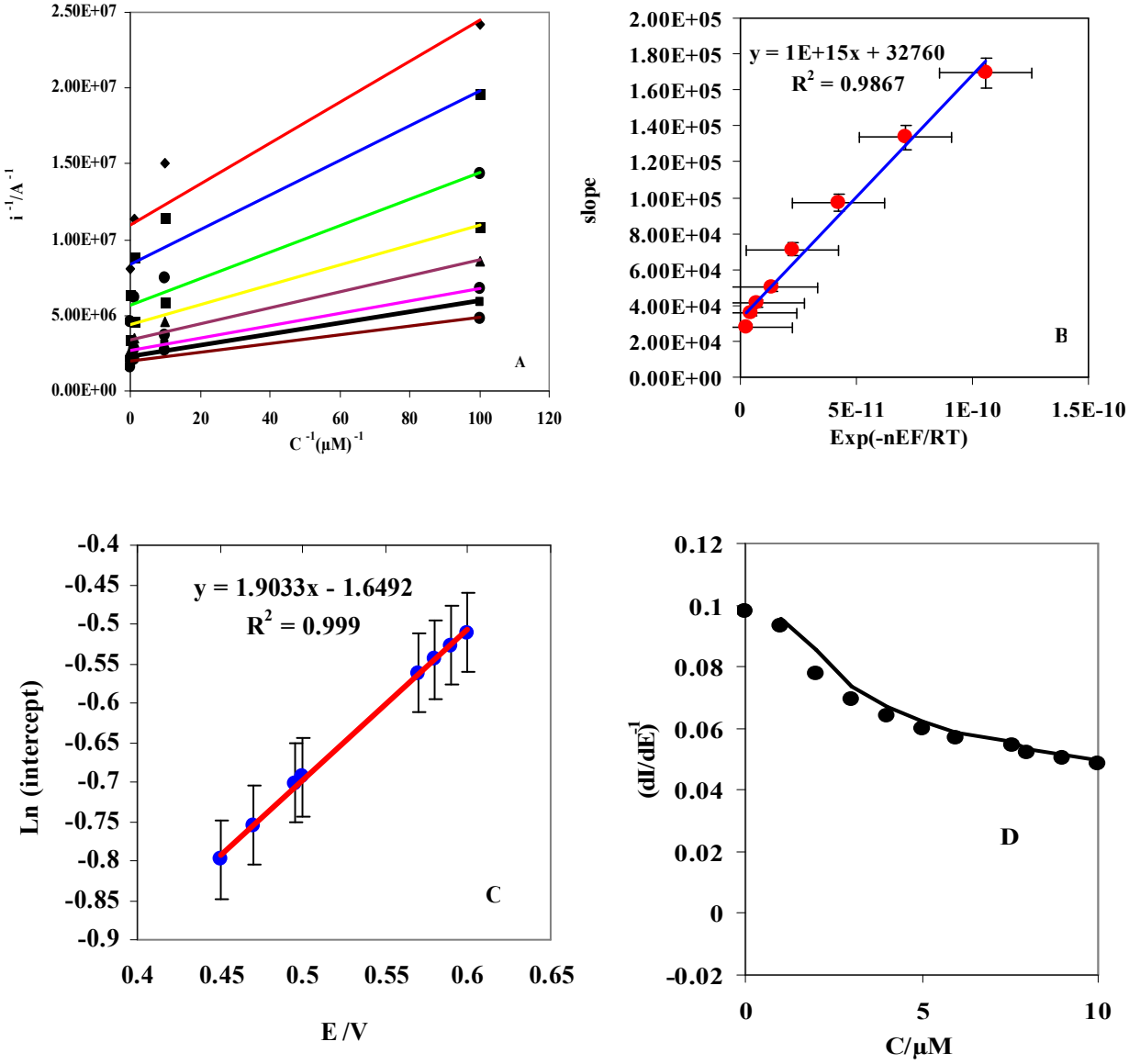

Fig. 9

View Article Online
DOI: 10.1039/C3RA42393J

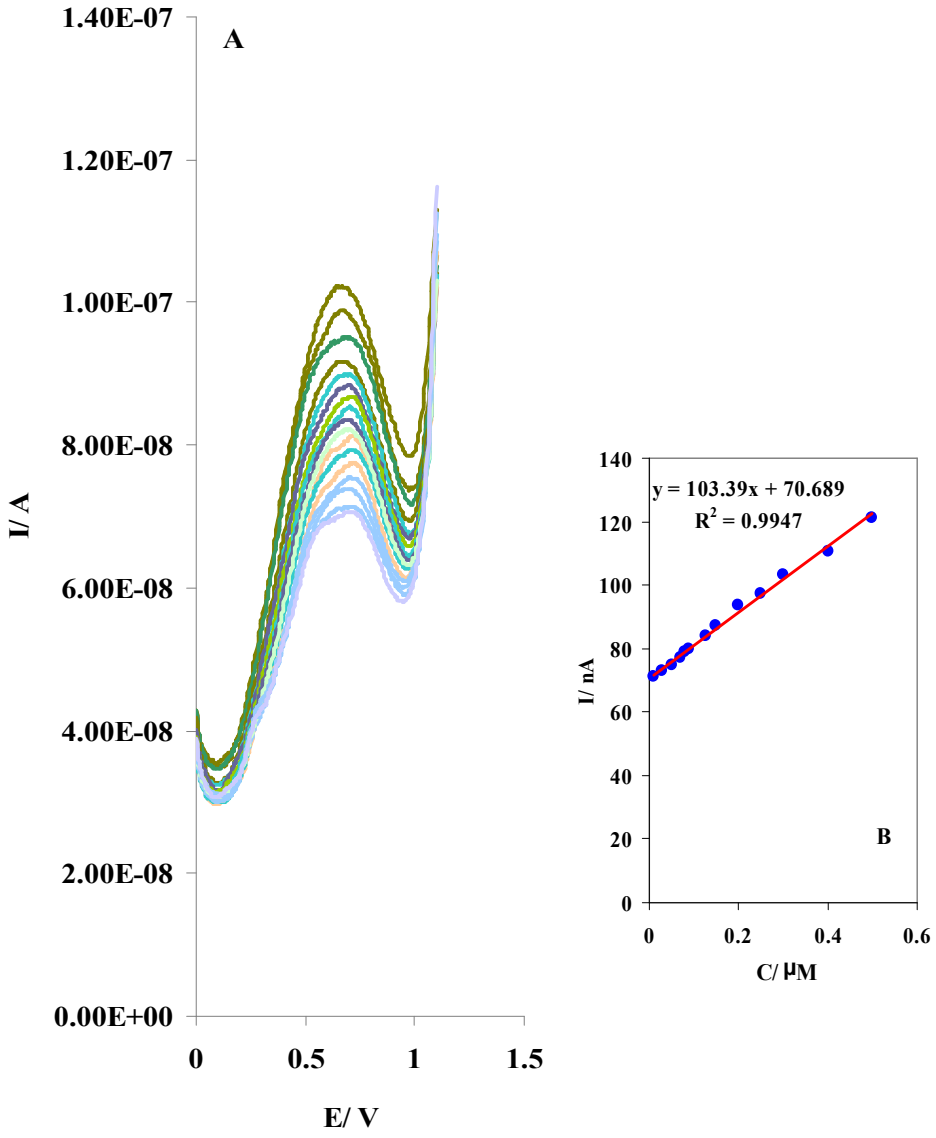

Fig. 10

View Article Online
DOI: 10.1039/C3RA42393J

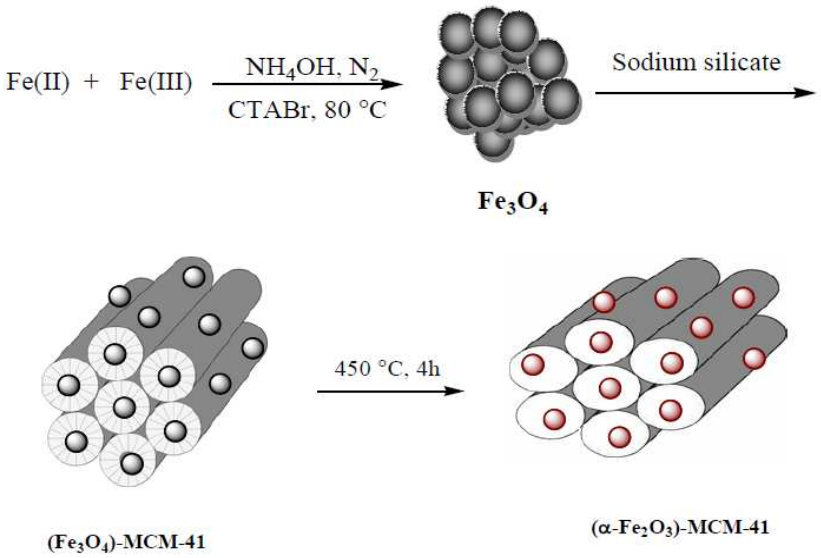

Scheme 1

View Article Online
DOI: 10.1039/C3RA42393J

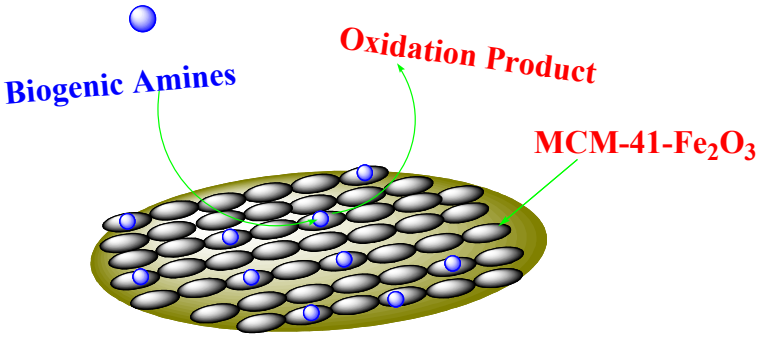

Scheme 2

View Article Online
DOI: 10.1039/C3RA42393J

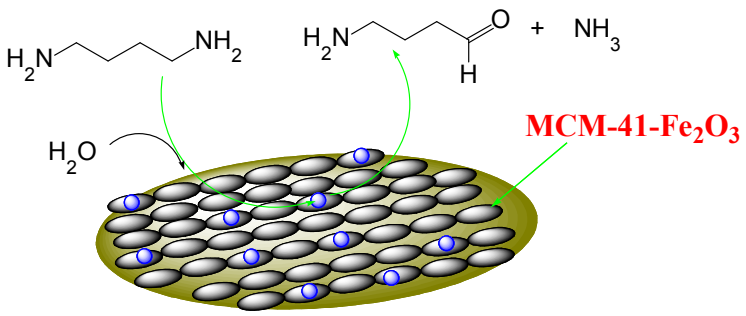

A

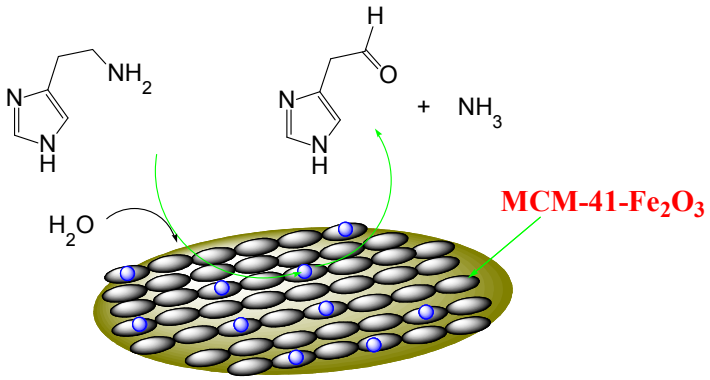

B

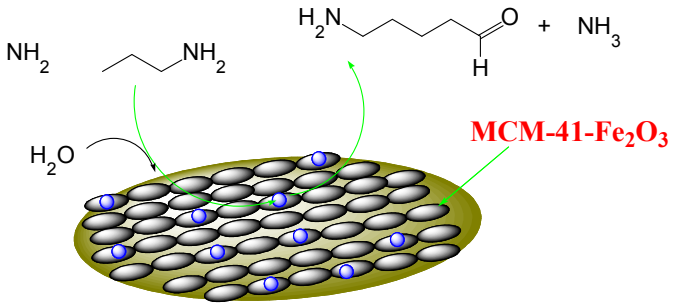

C

Scheme 3